CHEMICAL ENGINEERING TRANSACTIONS
VOL. 86, 2021
A publication of AIDIC
The Italian Association of Chemical Engineering
Online at www.cetjournal.it
Guest Editors: Sauro Pierucci, Jiří Jaromír Klemeš

ISBN 978-88-95608-84-6; **ISSN** 2283-9216

CFD-DEM analysis of the two-phase flow and particle dispersion in carrier-based Dry Powder Inhalers

Francesca O. Alfano[a,*], Andrea Benassi[b,c], Roberto Gaspari[b], Alberto Di Renzo[a], Francesco P. Di Maio[a]

[a]Dipartimento DIMES, Università della Calabria, Rende (CS), Italy
[b]DP Manufacturing & Innovation, Chiesi Farmaceutici SpA, Parma, Italy
[c]International School for Advanced Studies (SISSA), Trieste, Italy
francesca.alfano@unical.it

Fine particle lift and dispersion by gas flows is utilized as specialized technology in pharmaceutical devices such as Dry Powder Inhalers (DPI), where the fine API (Active Pharmaceutical Ingredient) is delivered after aerosolization as a result of the complex interplay between adhesive, impact and hydrodynamic forces. In the present contribution, Computational Fluid Dynamics and Discrete Element Method coupled simulations (CFD-DEM) are used to compute the two-phase swirling flow field in a DPI. The capability of the CFD-DEM model to represent the transiently developing swirl flow and stability is assessed in a simplified inhaler geometry. The trajectories and velocity profiles of the particles are investigated first in carrier-only systems, quantifying flow patterns, local solids distribution and expulsion rate. DEM with adhesive forces and rolling friction is then used to reproduce the deaggregation during inhalation. The proportion of detached API is studied by characterizing the trajectories, expulsion patterns and force balances, providing valuable insight into the microscopic mechanisms responsible for the macroscopic behaviour.

1. Introduction

Dry powder inhalers (DPI) are medical devices specifically engineered to ensure maximum and effective delivery of active pharmaceutical ingredients (API) in powder form upon inhalation by a patient. They are commonly applied for the treatment of respiratory diseases such as asthma and COPD and are being assessed in other areas such as antibiotic therapies or vaccination campaigns (Hoppentocht et al., 2014). The advantages of DPI compared to other inhalation therapies are: absence of propellants, quick drug administration, ease of use, no coordination required, multi-dose devices available (Berkenfeld et al., 2015). Also, the activation of the aerodispersion process by the patient's breath facilitates the powder uptake through the respiratory system (Islam and Gladki, 2008). These devices have attracted a growing interest in the last few years and much effort is being devoted to their most efficient design and the optimal corresponding powder formulation. In carrier-based dry powder inhalers, relatively coarse carrier particles (100 to 400 μm) are dry coated, i.e. surrounded, by adhered fine API powder (1 to 5 μm). The carrier guarantees better flowing properties and avoids the formation of API agglomerates (Pilcer et al., 2012). Before leaving the device, the API particles should detach from the carrier, to become freely transported all the way through to the patient's alveoli. The complex interaction between air flow, particle motion and adhesion/cohesion forces among API and carrier particles requires a very careful formulation and manufacture of dry coated particles along with an optimal device geometry and flow configuration. The understanding of these factors and the ability to manipulate them is crucial to the achievement of the desired drug delivery (van Wachem et al, 2017). In helping the development of increasingly effective devices, numerical simulation tools can be a valuable ally. Computational fluid dynamics (CFD) is widely used in the design of different types of inhalation devices to determine aerodynamic paths and turbulent flow effects (Sommerfeld et al, 2018) while Lagrangian approaches, such as DEM (Discrete Element Modelling), can be a powerful tool to study the solid phases, due to the detailed treatment of particle-particle and particle-wall contacts

and the possibility to study dense system with a 4-way coupling approach (Tong et al., 2015). In this work, a 4-way coupled, CFD-DEM model is used to simulate the detailed fluid and particle flow fields in a carrier-based dry powder inhaler with the aim to examine the behaviour of the carrier particles lifted by the swirling air flow, characterise the evolution of the carrier particle discharge during dose expulsion and investigate the dynamics of cohesive dry coated particles.

2. Methodology

The two-phase hydrodynamics is modelled according to the CFD-DEM approach (Norouzi et al., 2016), using the open-source code MFIX-DEM (version 18.1.5) and extended features. Basic details of the physical model and computational methods can be found in the documentation available on the website (Garg et al., 2012).
The contact model adopted is the non-linear Hertz-Mindlin no-slip model (Di Renzo and Di Maio, 2004). The cohesive/adhesive force between the like or dissimilar particles and with the walls are accounted for using a combination of a van der Waal's force model between distant particles and constant surface energy model for particles in contact, reading:

$$F_{coh} = \begin{cases} 4\pi\gamma R_{eq} & \text{for contacting particles} \\ \frac{24\pi z_{in}^2 \gamma R_{eq}}{d_{AP}^2} & \text{for non} - \text{contacting particles} \end{cases} \quad (1)$$

where d_{AP} is the distance between the two particles involved, R_{eq} is the effective radius, z_{in} is the cut-off distance and γ is the surface energy. The particle-fluid interaction is taken into account through the Gidaspow-blend drag model (Lundberg et al., 2008). The original MFIX-DEM code has been modified and extended through user-defined functions: the solid phase timestep has been calculated according to Di Renzo and Di Maio (2004), and a rolling friction model, based on the constant directional torque (CDT) approach, has been implemented (Ai et al, 2011).

3. Geometry and model setup

The geometry of the considered inhaler is similar to the internal shape of the commercial device NEXThaler® (Corradi et al., 2014) and consists of three sections: a **dose cup**, at the bottom, that houses the initial dose of drug product, a **swirl chamber**, in which the air flow initially develops and a cylindrical **exit duct** on top of it. Top and side views and a 3D transparent representation of the geometry are reported in Figure 1. In the software, the geometry is imported from a triangulated STL file of the device boundaries. The DEM part of the code uses the triangular elements of the CAD file for collision detection and force calculations. In the definition of the Eulerian grid for the gas, MFIX uses the Cartesian grid cut cell technique (Dietiker et al., 2013). As the CFD-DEM method is a 4-way coupled, unresolved approach, particular attention needs to be paid to the grid size. Generally, $\Delta x/d_p > 2$ is suggested (Fullmer et al., 2018), with Δx being the characteristic cell size and d_p the particle diameter. Since the local-to-mesh variable interpolation method in MFIX (Garg et al., 2012) allows looser restrictions than centered volume fraction methods (Volk et al., 2018), a characteristic dimension of 250 µm for the cubical cells has been selected for use with both 150 and 200 µm particles, leading to a mesh composed by about 135k cells.

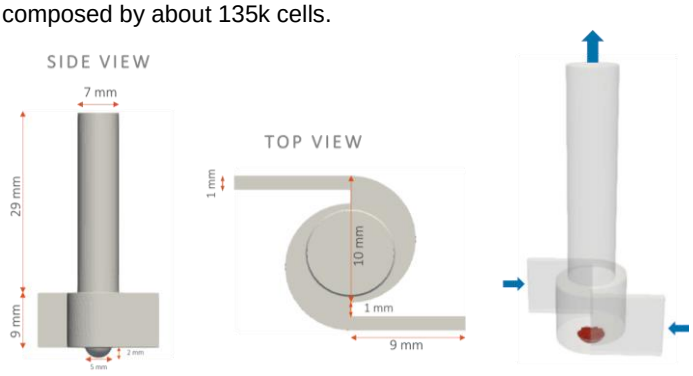

Figure 1: Geometry of the system. Side view, top view and transparent representation (with inlet and outlet sections highlighted). The red part represents the particles filling the hemispherical dose cup.

The simulated fluid is air at 25°C under conditions of incompressible flow. A volume flowrate boundary condition is applied to the two tangential inlets, from which a total of 60 l/min of air enter the system. A constant pressure condition is set to the outlet section. The powder consists of 10 mg of spherical particles. In some of the

simulations two solid phases are considered (both coarse carrier and fine API particles). The physical and mechanical properties of the solid phases are reported in Table 1. The initial velocity of the fluid and its gauge pressure in the transient simulations are zero. Particles are housed in the hemispherical cup placed under the swirl chamber, achieved by a DEM-only gravity settling simulation. The simulations have been carried out on a hybrid HPC cluster available at the CheProDes laboratory (University of Calabria). Parallel processing of the calculations based on MPI has been extensively used by running the code on multiple cores (up to 64).

Table 1: Physical and mechanical properties used in the simulations.

	Carrier	API
Number of particles	3422 - 1579	136322
Diameter, d [μm]	150 - 200	10
Particle density, ρ [kg/m^3]	1500	1400
Young modulus, E [GPa]	0.2	0.2
Poisson ratio, ν [-]	0.45	0.45
Restitution coefficient, e [-]	0.2	0.2
Friction coefficient, μ_s [-]	0.5	0.5
Rolling friction coefficient, μ_r [-]	0.3	0.3
Surface energy density, γ [J/m^2]	0.004	0.004

4. Results and discussion

4.1 Single-phase fluid field

The velocity field, in terms of magnitude, resulting from a fluid-only simulation after 50 ms is reported in Figure 2. The streamlines in the rightmost 3D representation show the horizontal inlet flow that leads to the formation of a rotational flow in the swirl chamber. The peculiar shifted half circular walls of the swirl chamber resemble those of a two-inlet cyclone and, due to the symmetry, produce an internal circular flow with a vertical component directed upwards, as shown by the helical shape of the streamlines in the exit duct. The flow appears rather developed in both the swirl chamber and the exit duct. In the transition zone, corresponding to the restriction of the vertical cross-sectional area, the highest velocities are observed reaching values above 40 m/s. In the swirl chamber, the tangential velocity is found to reach higher values than in the exit duct, as shown in the x-coordinate profile. Development of the steady-state flow field occurs in a short time (about 10 ms), also due to the inlet boundary condition instantaneously set to 60 l/min.

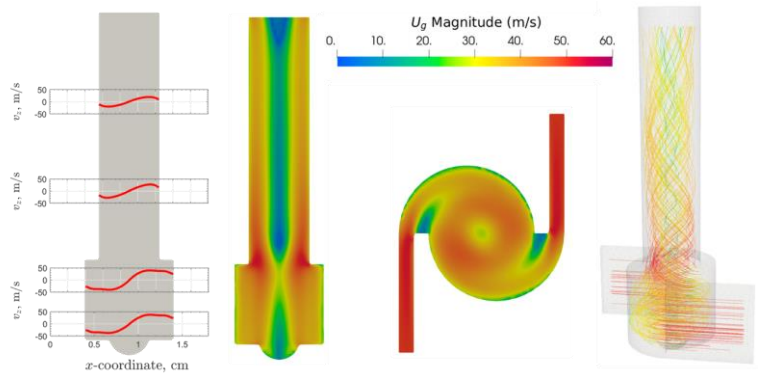

Figure 2: Velocity field of the fluid flow inside the device: horizontal component of velocity profiles (v_z) at different vertical coordinates, side view and top view of gas velocity magnitude, streamlines (flowrate 60 l/min).

4.2 Analysis of the carrier motion

Two-phase flow involving free flowing carrier particles has been simulated for 500 ms to examine particle trajectories. 3422 carrier particles with a 150 μm diameter (corresponding to 10 mg of powder) have been considered. Figure 3 shows the evolution of the particle positions and velocity magnitude. Even before the full development of the gas flow, the swirling gas motion acts almost immediately on the powder, which is raised upwards, forming a dense central fountain of particles surrounded by looser solid flow (see 0.005 and 0.008 s

frames), in which particles are pushed radially outwards by the centrifugal motion. When the fluid reaches the steady state, nearly all the particles have been lifted from the cup and most of them rotate in the swirl chamber below the swirl chamber ”ceiling”, just close to the exit duct (see 0.015 and 0.5 s frames).

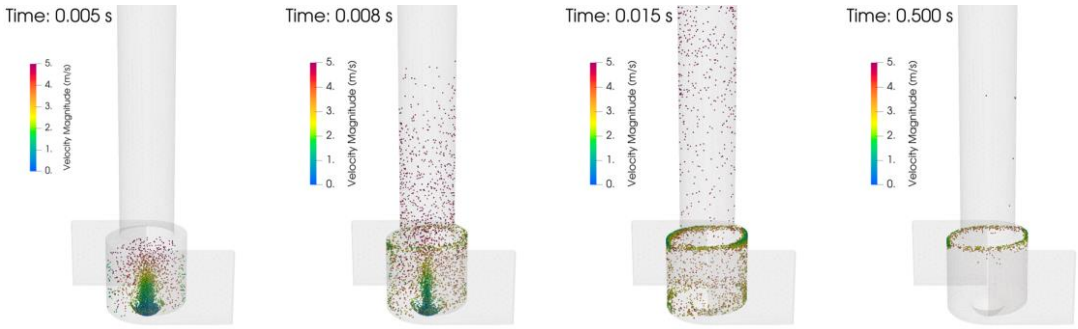

Figure 3: Carrier position during the simulation.

In quantitative terms, the exit profile of the particles can be examined as the percent of solid leaving the device in time (Figure 4). Three different emission stages can be identified: a steep growth is observed until 0.02 s; another linear, weaker trend characterizes the exit profile until 0.11 s; after that, the number of particles leaving the system follows a gently increasing trend until, at the end of the simulation (0.5 s), the percentage of delivered particles reaches about 84%. By comparing the particles emitted with the particle trajectories shown in Figure 3, it can be concluded that the first steep stage corresponds to particles lifted which exit essentially without contact with the walls; in the second stage, particles leave the device in a helical motion; in the third stage, the particles leaving the system are picked up progressively by the group of the ones rotating below the swirl chamber ceiling, whose gradual erosion yields a lower emission rate.

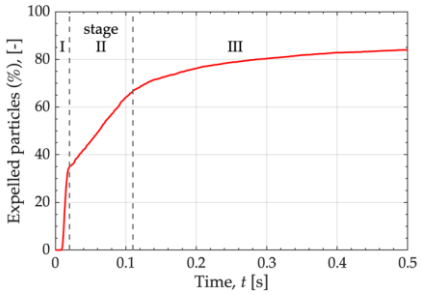

Figure 4: Cumulative percentage of expelled particles as a function of time (60 l/min, 150 µm particles)

The peculiar formations of particles hovering around in the swirling chamber before leaving can be effectively used for validation purposes. Indeed, it was observed in commercially available DPI by Pasquali et al. (2015), who conducted experimental analysis by laser illuminated high speed imaging on Chiesi’s Nexthaler®. As shown in Figure 5, in both experiments and simulations, most of the particles are located in the upper part of the swirl chamber.

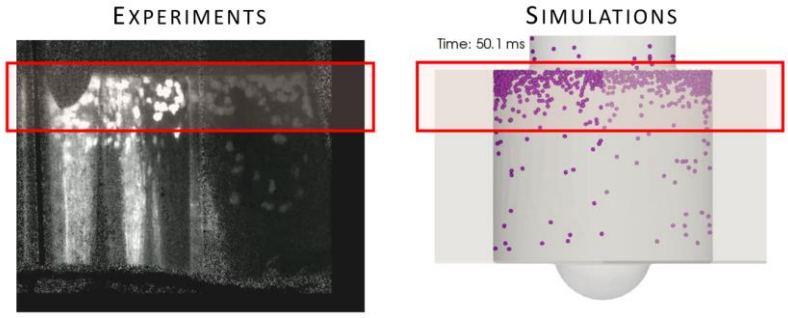

Figure 5: Position of the particles in the swirl chamber after 50 ms in experiments and simulations.

4.3 Dispersion of API particles

The combined simulation of the fine API together with the coarse carrier is extremely challenging, as the size difference requires a high number of contacting particles to be handled and very small time-step (~10^{-8}–10^{-9} s). Yet, it is a key ingredient to study in detail the fines' deaggregation process. In this work, the explicit aerodispersion of a two-component system consisting of 200 μm carrier particles dry coated by 10 μm API particles has been studied. 10 mg of powder is considered, with a 1% (w/w) of API particles. Fine particles are placed on carrier particle according to a random configuration fulfilling a prescribed percent coverage. To achieve the desired dosage, there are ~1600 carrier particles, each covered with about 86 API particles. As shown by Begat et al. (2004), the cohesive (drug-drug) and adhesive (drug-excipient) interaction properties play a significant role in the homogeneity of the blend and the deaggregation and dispersion properties of the respirable particles. For the cohesion/adhesion model utilized (see Eq (1)) appropriate parameters have been used by referring to the work of Cui et al. (2014), who determined the pull-off force between untreated glass beads and spray dried salbutamol sulphate particles via AFM measurements. The reported value of the force ($2.58 \cdot 10^{-7}$ N) has been set to calculate the surface energy, γ, whose value is reported in Table 1. This force is about 10^5 times stronger than the weight of the considered API particle.

Figure 6a shows the configuration of the two solid phases during the first 15 ms of the simulation. The path followed by API particles shows that they get relatively easily deaggregated by the carrier particles. Then they are lifted before the carrier particles, following a similar pattern as observed with just carrier particles, i.e. a central dense, fountain-like, region around the axis with the rest of particles being pushed laterally on the swirl chamber walls. After 3 ms, the first few API particles enter the inhalation duct. After 7 ms the API particles have formed a helical dense flow towards the exit and the first few carrier particles enter the inhalation duct. After 10 ms the particles are fully dispersed throughout the device and the carrier particles show again the tendency to accumulate near the swirl chamber ceiling, as visible in the 15 snapshot.

The time evolution of the release is shown in the higher plot in Figure 6b separately for API and carrier particles. Once the API particles detach from the carrier, their characteristic time for release is expectedly shorter. Carrier particles' release follows the pattern already discussed in the previous sections. The early detachment causes a substantial release of API particles, but not all of them. The API particles exposed to the surface, i.e. to the direct action of the fluid are lifted almost immediately, while other ones are peeled during carrier particle lift off. As shown by the average number of attached API particles to carrier, reported in the lower plot in Figure 6b, there is an initial drop from 86 to 60 API particles attached to the carrier after around 2 ms, essentially owing to the hydrodynamic interactions in the dense region. This is followed by a gradual decrease of the average number of API still in the aggregated state, which later detach, likely as a result of particle-particle and particularly particle-wall impacts.

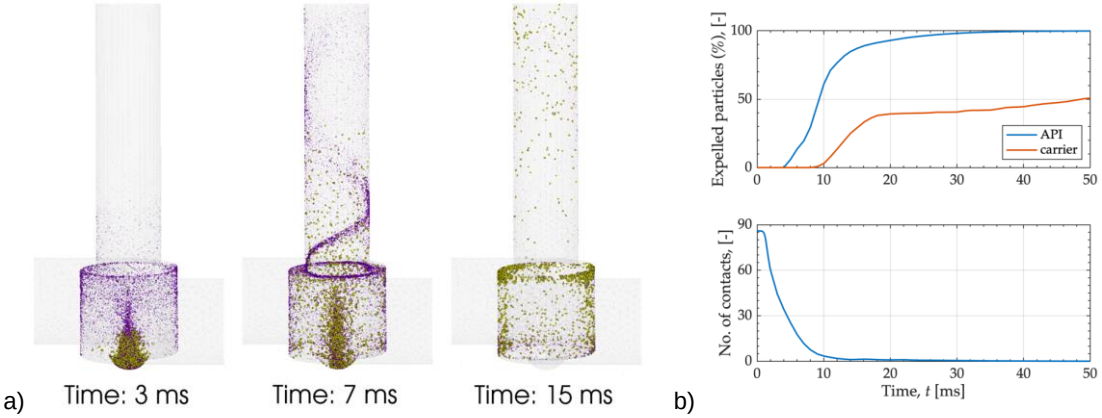

Figure 6: a) position of carrier (green) and API (purple) particles during the simulation; (b) exit profiles of API and carrier particles and average number of API particles attached to carrier particles as a function of time.

5. Conclusions

The air and particle hydrodynamics in dry powder inhalers have been investigated in detail, with specific interest in the mechanisms responsible for carrier particle lift, motion and delivery and API particle deaggregation in a representative device configuration. The analysis shows that the transient air flow development is extremely quick and, without particles, steady-state is achieved in about 10 ms, with swirling flow in the lower chamber. In the conditions considered, the solids outflow from the device follows three stages, accounting for: up to 35% of

the initial mass directly flowing out without contact with walls (stage I), up to 66% after helical flow (stage II) and a final, slower outflow after several looping in the swirling chamber, totaling about 84% of expelled solids (stage III) after 0.5 s. The occurrence of the annular motion in the swirl chamber is confirmed by experiments available in the literature.

Challenging CFD-DEM simulations on API-coated carrier particles were carried out considering an API-carrier size ratio of 1 to 20 and a 1% w/w loading. DEM allows tracking all API particles during their initial lift off, some still attached to the carrier particles, other ones already deaggregated. Overall, the simulations provide a quantitative description of the flow characteristics of the solids and help to identify specific responsibility for the observed macroscopic behaviour of the device during dose delivery.

Acknowledgments

The partial support to the research from Chiesi Farmaceutici is gratefully acknowledged.

References

Ai, J., Chen, J. F., Rotter, J. M., & Ooi, J. Y. (2011). Assessment of rolling resistance models in discrete element simulations. Powder Technology, 206(3), 269-282.

Begat, P., Morton, D. A., Staniforth, J. N., & Price, R. (2004). The cohesive-adhesive balances in dry powder inhaler formulations II: influence on fine particle delivery characteristics. Pharmaceutical Research, 21(10), 1826-1833.

Berkenfeld, K., Lamprecht, A., & McConville, J. T. (2015). Devices for dry powder drug delivery to the lung. Aaps Pharmscitech, 16(3), 479-490.

Corradi, M., Chrystyn, H., Cosio, B. G., Pirozynski, M., Loukides, S., Louis, R., & Usmani, O. S. (2014). NEXThaler, an innovative dry powder inhaler delivering an extrafine fixed combination of beclometasone and formoterol to treat large and small airways in asthma. Expert Opinion on Drug Delivery, 11(9), 1497-1506.

Cui, Y., Schmalfuß, S., Zellnitz, S., Sommerfeld, M., & Urbanetz, N. (2014). Towards the optimisation and adaptation of dry powder inhalers. International Journal of Pharmaceutics, 470(1-2), 120-132.

Di Renzo, A., & Di Maio, F. P. (2004). Comparison of contact-force models for the simulation of collisions in DEM-based granular flow codes. Chemical engineering science, 59(3), 525-541.

Dietiker, J. F., Li, T., Garg, R., & Shahnam, M. (2013). Cartesian grid simulations of gas–solids flow systems with complex geometry. Powder Technology, 235, 696-705.

Fullmer, W. D., & Musser, J. (2018). CFD-DEM solution verification: Fixed-bed studies. Powder Technology, 339, 760-764.

Garg, R., Galvin, J., Li, T., & Pannala, S. (2012). Documentation of open-source MFIX–DEM software for gas–solids flows, From URL https://mfix.netl.doe.gov/documentation/demdoc2012-1.pdf.

Hoppentocht, M., Hagedoorn, P., Frijlink, H. W., & De Boer, A. H. (2014). Technological and practical challenges of dry powder inhalers and formulations. Advanced Drug Delivery Reviews, 75, 18-31.

Islam, N., & Gladki, E. (2008). Dry powder inhalers (DPIs)—a review of device reliability and innovation. International Journal of Pharmaceutics, 360(1-2), 1-11.

Lundberg, J., & Halvorsen, B. M. (2008). A review of some existing drag models describing the interaction between phases in a bubbling fluidized bed. In Proc. 49th Scand. Conf. Simulation and Modeling, Oslo University College, Oslo, Norway (pp. 7-8).

Norouzi, H. R., Zarghami, R., Sotudeh-Gharebagh, R., & Mostoufi, N. (2016). Coupled CFD-DEM modeling: formulation, implementation and application to multiphase flows. John Wiley & Sons.

Pasquali, I., Merusi, C., Brambilla, G., Long, E. J., Hargrave, G. K., & Versteeg, H. K. (2015). Optical diagnostics study of air flow and powder fluidisation in Nexthaler®—Part I: Studies with lactose placebo formulation. International Journal of Pharmaceutics, 496(2), 780-791.

Pilcer, G., Wauthoz, N., & Amighi, K. (2012). Lactose characteristics and the generation of the aerosol. Advanced Drug Delivery Reviews, 64(3), 233-256.

Sommerfeld, M., Cui, Y., & Schmalfuß, S. (2019). Potential and constraints for the application of CFD combined with Lagrangian particle tracking to dry powder inhalers. European Journal of Pharmaceutical Sciences, 128, 299-324.

Tong, Z., Yu, A., Chan, H. K., & Yang, R. (2015). Discrete modelling of powder dispersion in dry powder inhalers-a brief review. Current Pharmaceutical Design, 21(27), 3966-3973.

van Wachem, B., Thalberg, K., Remmelgas, J., & Niklasson-Björn, I. (2017). Simulation of dry powder inhalers: combining micro-scale, meso-scale and macro-scale modeling. AIChE Journal, 63(2), 501-516.

Volk, A., Ghia, U., & Liu, G. R. (2018). Assessment of CFD-DEM solution error against computational cell size for flows through a fixed-bed of binary-sized particles. Powder Technology, 325, 519-529.